Petroleum Science 20 (2023) 48–59

Contents lists available at ScienceDirect

Petroleum Science

journal homepage: www.keaipublishing.com/en/journals/petroleum-science

Original Paper

Paleoenvironment reconstruction of the Middle Ordovician thick carbonate from western Ordos Basin, China

Jia-Qi Yang [a, b], Jun-Tao Zhang [b], Zhi-Liang He [c, *], Tao Zhang [b]

[a] School of Energy Resources, China University of Geosciences, Beijing, 100083, China
[b] SINOPEC Exploration and Production Research Institute, Beijing, 100083, China
[c] China Petrochemical Corporation Ltd., Beijing, 100728, China

ARTICLE INFO

Article history:
Received 8 February 2022
Received in revised form
3 August 2022
Accepted 23 August 2022
Available online 28 August 2022

Edited by Jie Hao and Teng Zhu

Keywords:
Middle darriwilian isotope carbon excursion
Paleoenvironment
Natural gas exploration
Middle ordovician
Ordos basin

ABSTRACT

Reconstructing paleoenvironments has long been considered a vital component for understanding the development and evolution of carbonate reservoirs. The Middle Ordovician Period is considered the archetypical greenhouse interval, and also a critical period in biological evolution. The Middle Darriwilian isotope carbon excursion has been observed in many areas of the world and may be related to the biological explosions caused by decreases in the temperature. The thick carbonate rocks in the fifth member of the Middle Ordovician Majiagou Formation in the Dingbei area of the Ordos Basin were chosen as an example, based on the concentration of major, trace and rare earth elements as well as C, O and Sr isotopic analyses, the paleoenvironment was reconstructed. And its impact on natural gas exploration was analyzed. The results show that the seawater paleotemperature was 29 °C, suboxic-anoxic paleoredox conditions were observed, and the seawater paleosalinity was high. A large number of plankton in the biological explosion caused a rapid increase in the total organic carbon in carbonate rocks, which provided natural gas as supplemental source rocks. Affected by early meteoric water, the dissolution of gypsum laid the foundation for high-quality reservoirs, and the residual gypsum also further preserved natural gas. This study provides new data for the paleoenvironment and a theoretical basis for further natural gas exploration.

1. Introduction

Petroleum is an essential driver for human societies development (Wang et al., 2022a; 2022b), recently, a set of important carbonate reservoirs are developed in the Majiagou Formation of the Middle Ordovician in the Ordos Basin (e.g., Fu et al., 2019; He et al., 2020; He et al., 2021). Numerous research has been conducted on reservoir characteristics (Yu and Cui, 2019), development mechanism (Zhang et al., 2016, 2017), and evolution model (Xiao et al., 2021; Xiong et al., 2022). The development of carbonate rocks is severely restricted by the paleoenvironment, especially in the mixed depositional model of evaporite and carbonate rocks developed in the study area (Xiao et al., 2021). However, little work has been done on the paleoenvironment reconstruction of the Middle Ordovician in the Ordos Basin, which severely restricted the research on carbonate rock development and evolution.

The Ordovician is an important geological period of tectonic climate and biological evolution in the Early Paleozoic. The seawater temperatures reached a maximum of 45 °C in the early Ordovician, but gradually dropped to about 23 °C in the late period (e.g., Sepkoski, 1995; Dixon et al., 2001). Climate change may be an important factor leading to biological evolution (Haq and Schutter, 2008; Young et al., 2010; Pohl et al., 2014). Three biological radiations developed during the Ordovician, which are collectively referred to as the Great Ordovician Biodiversification Event (Trotter et al., 2008; Zhang et al., 2010; Chen, 2019; Danelian and Monnet; 2021). These events were not like the Cambrian one, while the biological species and genera in this period became increasingly "lush" (Webby et al., 2004). Severe climate change had a serious impact on biological evolution, thus, studying the Ordovician paleoenvironment is particularly important.

The inorganic carbon isotopic chemical stratigraphy of carbonate rocks has the potential for global stratigraphic correlation (Ren et al., 2017; Chen, 2019). Although the value of the C-isotopes ($\delta^{13}C$)

* Corresponding author.
E-mail address: hezhiliang@sinopec.com (Z.-L. He).

https://doi.org/10.1016/j.petsci.2022.08.027

may change to a certain extent when affected by some regional factors, for global isotopic changes such as the $\delta^{13}C$ excursion, the overall evolution trend is clear. During the Middle Ordovician, at approximately 464–466 Ma (Goldman et al., 2020), a $\delta^{13}C$ excursion has been observed in many areas around the world, which has been named the Middle Darriwilian isotope carbon excursion (MDICE) and has received extensive attention (Schmitz et al., 2010; Albanesi et al., 2013; Calner et al., 2014; Kah et al., 2016; Young et al., 2016; Henderson et al., 2018; Bergström et al., 2020; Danelian and Monnet, 2021). This phenomenon was first recognized in Baltoscandia by Ainsaar et al. (2004) and Meidla et al. (2004). Then, the same excursion was seen in South China (e.g., Schmitz et al., 2010; Zhang et al., 2010), North America (e.g., Leslie et al., 2011; Young et al., 2016), South America (Albanesi et al., 2013), and other areas. The MDICE presents from −2.0‰ in the Dapingian to approximately +1.0‰ in the Middle Darriwilian (Dw2-Dw3), and the $\delta^{13}C$ increases almost monotonically, except for an abrupt negative peak at the base of the Dw2 stage slice (cf. Wu et al., 2018).

The Ordos Basin is one of the areas with relatively complete development and exposure of the Early–Middle Ordovician strata in the North China Platform (Qiang, 2019). Previous studies have involved systematic research on oil and gas geology in this area (Zhang et al., 2016, 2017; Wang et al., 2020); however, there are relatively fewer studies on the evolution of paleoenvironment, particularly in the Dingbei area. This study (a) provides new data for petrography, elements, and REE concentrations to restrict the paleoenvironment; (b) provides an understanding of paleoenvironmental control for the MDICE caused by a biological explosion in the Early Paleozoic; and (c) further explains the influence of the MDICE event on natural gas exploration.

2. Geological backgrounds

The Ordos Basin, which is the second largest sedimentary basin and one of the three largest carbonate basins in China, is rich in natural gas resources (Wang et al., 2020). This basin is located in the western region of the North China Platform, with a total area of 25×10^4 km^2 (Su et al., 2012; Xie et al., 2020), and it can be divided into the Yimeng Uplift, the Weibei Uplift, the Jinxi Fault–Fold Belt, the Yishan Slope, the Tianhuan Syncline and the Fault–Fold Belt of the Western Margin 6 structural units (Fig. 1).

The Majiagou Formation comprises carbonate rocks deposited in the main part of the Ordos Basin and generally has several hundred meters thick deposits. It is divided into 6 members that recorded changes in sea level, with the second member (Ma2 Fm.), fourth member (Ma4 Fm.), and sixth member (Ma6 Fm.) representing transgressive episodes, and the first member (Ma1 Fm.), third member (Ma3 Fm.), and fifth member (Ma5 Fm.) representing regressive episodes (Yang, 2011; He et al., 2013). Affected by high temperatures, as the Ordos Basin was near the equator during the Middle Ordovician, a large number of gypsum rocks were co-deposited with carbonate rocks during regression (Fig. 1).

The age of the Ma5 Fm. is constrained to the Dapingian-Darriwilian by the correlation of regional biostratigraphy (Wang et al., 2015; Zhao et al., 2015; Zhang et al., 2019). The biostratigraphy (*L. variabilis* and *E. suecicus*) corresponds to the Dw2 (An and Zheng, 1990). During the end of Darriwilian and Sandbian, the largest volcanic activity was recorded by an approximately 50 cm thick volcanic tuff, which was widely distributed in the western and southern basin (e.g., Zhao et al., 2015).

There are two sets of source rocks developed in the basin: coal-bearing source rocks in the upper Paleozoic and carbonate rocks in the lower Paleozoic. The former exhibits relatively high total organic carbon (TOC), maturity, and natural gas generation intensity compared with the carbonate rocks (Tu et al., 2016; Li et al., 2017). The lower Paleozoic carbonate rocks can only provide natural gas as supplemental source rocks (Qi and Guo, 2017; Xu et al., 2021). Many types of reservoirs are developed in the Majiagou Formation, including karst (Xiong et al., 2016), subsalt dolomite (Fu et al., 2019), and limestone fracture reservoirs (Shu et al., 2021). Mudstone developed in the Benxi and Taiyuan Formations, as direct caps, cover the karst reservoir of Ma5 Fm., which plays a significant role in protecting the underlying reservoirs. The deposited gypsum strata can also promote natural gas sealing (Qi and Guo, 2017).

3. Methods

The petrological characteristics of samples were observed and described using a microscope at the SINOPEC's Key Laboratory for Petroleum Reservoir, China. The compositions of major and trace elements; REEs and C, O and Sr isotopes were analyzed at the Beijing Research Institute of Uranium Geology, China. Relatively pure carbonate rock samples were obtained using a drilling bit with a diameter of approximately 0.5 mm. Micro drilling samples were obtained for portions without non-carbonate minerals before conducting various experimental pretreatments.

A PerkinElmer 5300DV ICP–OES was used for the analysis of major elements. After the bulk samples were ground into powder, samples were heated at 1000 °C for 1 h, the excess materials were dissolved by HNO_3, HCl, and HF, and the contents of major elements (including Ca, Mg, Fe, Mn, and Si) were determined. The trace elements were conducted on a PerkinElmer Nexion300D ICP-MS instrument, samples were digested in a mixture of nitric acid and hydrofluoric acid at 185 °C for 24 h. And measured Sr, Zr, Hf, Ti, Sc, Th, and other trace elements (the specific elements are shown in Table 1). We analyzed the REEs using the dissolution methods of Chen et al. (2013) to avoid the influence of non-carbonate minerals components. The samples were ground into a 200-mesh powder, before dissolving them with a mixture of nitric acid and hydrofluoric acid and testing the composition of REE + Y.

The stable C and O isotopic compositions of carbonate samples were also analyzed. The mentioned above samples were analyzed using a Finnigan MAT253 mass spectrometer. The treatment method was the same as that introduced in Lash (2018). The values of $\delta^{13}C$ and $\delta^{18}O$ are reported in δ per unit (‰) relative to the Vienna–Pee·Dee·Belemnite (V–PDB) standard and the Vienna Standard Mean Ocean Water (V–SMOW), respectively. The Chinese standards GBW04416 ($\delta^{13}C = +1.61 \pm 0.03$‰, V–PDB and $\delta^{18}O = -11.59 \pm 0.11$‰, V–PDB) and GBW04417 ($\delta^{13}C = -6.06 \pm 0.06$‰, V–PDB and $\delta^{18}O = -24.12 \pm 0.19$‰, V–PDB) were used as standard samples, and the calibration of these standard samples was performed by testing every five samples to ensure that the accuracy was better than 0.2‰.

Sr isotope tests were conducted on a Finnigan MAT Triton TI. Approximately 100 mg of carbonate rock materials were weighed (to 0.1 mg precision) into Savillex 7.5 mL Teflon-PFA vials. The samples were dissolved on a hotplate at 80 °C using 2.0 mL of 0.2 M HCl for 4 h. The sample solution is cooled to room temperature for 1 h before centrifugation for 8 min at 5000 rpm. Then, the supernatant is picked up from a centrifugation tube and dried on a hotplate. Next, the samples were re-dissolved with 1.0 mL of 2.5 M HCl. Then, the sample solution was loaded onto the preconditioned resin column with 2 mL of AG50W × 12 (200–400 mesh) for the separation of Sr from the sample matrix. After rinsing four times with 0.5 mL of 2.5 M HCl, the column was washed with 7 mL of 5 M HCl. Afterward, the Sr fraction was stripped with 3.5 mL of 5 M HCl (Li et al., 2019). The obtained $^{87}Sr/^{86}Sr$ ratio was compared to that of the NBS-987 standard sample ($^{87}Sr/^{86}Sr = 0.710273 \pm 0.000012$).

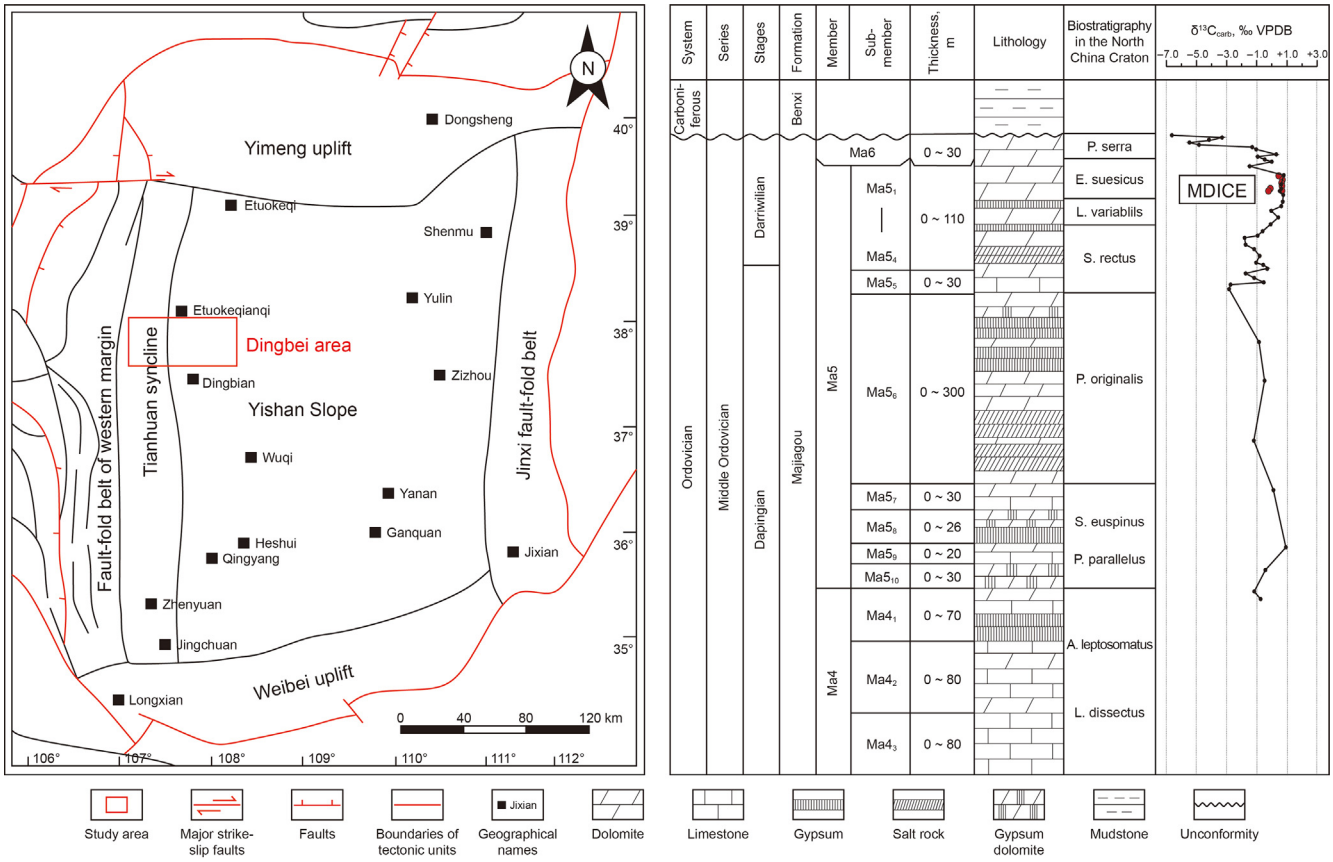

Fig. 1. Map showing the structural location and strata development of the Dingbei area in the Ordos Basin (the geochronological frame is from Zhao et al., 2015, An and Zheng, 1990; the red C isotope data were measured using samples in this study, and points shown in black are collected from He et al., 2014, Zhang et al., 2016, Cao et al., 2018, Yu and Cui, 2019, He et al., 2021).

Table 1
Major and trace element composition.

Sample	Depth, m	Major elements composition, %						Trace elements composition, ppm				
		CaO	MgO	FeO	MnO	Al	Ti	Ba	Zr	Hf	Sc	Th
DB18-4	4009.50	50.91	3.10	0.28	0.011	0.359	0.015	13.0	2.94	0.08	1.10	0.54
DB18-5	4008.52	29.72	21.67	0.29	0.015	0.431	0.015	13.2	3.26	0.12	0.87	0.49
DB5-10	3834.70	29.33	21.92	0.35	0.008	0.308	0.006	9.8	1.96	0.06	0.78	0.37
DB5-12	3830.85	28.77	22.62	0.10	0.012	0.309	0.011	5.6	1.68	0.06	0.49	0.29
DB8-8	4269.28	28.94	22.70	0.13	0.011	0.247	0.006	4.6	1.78	0.07	0.51	0.33
DB8-11	4270.49	38.46	13.73	0.10	0.006	0.435	0.012	11.7	2.26	0.08	0.67	0.49
DB10-4	3904.40	49.36	4.78	0.05	0.007	0.398	0.013	12.0	2.34	0.08	0.87	0.48

Sample	Depth, m	Trace elements composition, ppm									
		Rb	Ni	Cu	Pb	P	V	Cr	Co	U	Sr
DB18-4	4009.50	2.59	20.10	1.97	1.48	0.006	8.19	3.39	2.10	1.40	235.0
DB18-5	4008.52	3.56	12.20	2.68	5.09	0.035	13.60	3.55	1.51	1.04	90.4
DB5-10	3834.70	2.49	13.50	2.21	4.54	0.024	11.60	2.76	1.60	0.95	86.0
DB5-12	3830.85	1.76	11.00	1.38	0.74	0.006	13.50	2.99	0.99	0.54	60.8
DB8-8	4269.28	1.50	10.30	1.46	0.80	0.006	7.78	2.12	0.94	0.57	61.0
DB8-11	4270.49	3.35	15.00	2.20	1.33	0.008	9.46	3.51	1.47	0.54	146.0
DB10-4	3904.40	2.16	20.00	2.31	2.07	0.007	8.17	2.93	1.77	2.12	206.0

4. Results

4.1. Petrological characteristics

The lithology of the Ma5 Fm. in the Dingbei area are carbonate and gypsum rocks. Intraclast biomicritic micritic limestone (L1), silty dolomite (RD1), and fine crystalline dolomite (RD2) have been observed in the study area according to the standard established by Folk (1962) (Fig. 2).

Particles of L1 were relatively small, at only several microns. A large number of intraclasts and foraminifera were observed (Fig. 2a). Many mold pores, solution pores, and cracks were observed. The cracks were filled with secondary calcite and dolomite, and the filling crystals were large, typically greater than 200

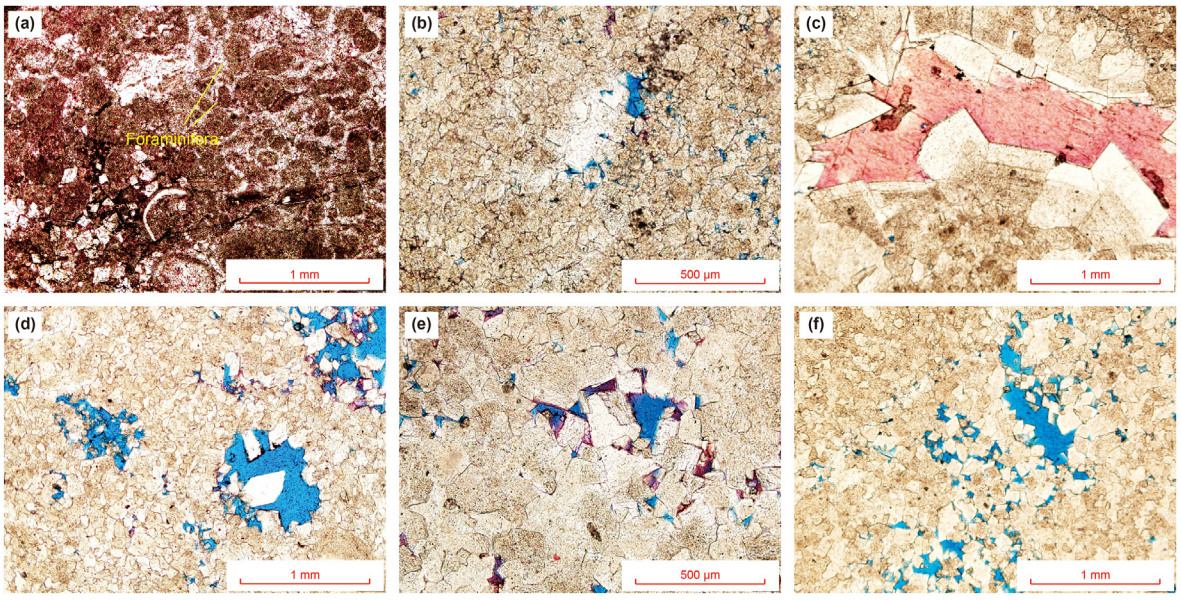

Fig. 2. Petrographic characteristics in the Dingbei area (a. intraclast biological micritic limestone, visible intraclast, and foraminifera, DB10-3; b. silty dolomite, secondary dolomite filled in the dissolution pore, DB5-11; c. silty dolomite, fracture filled with secondary calcite and dolomite, DB18-4; d. silty dolomite, secondary dolomite filled in the gypsum mold pore, DB9-2; e. fine crystalline dolomite, dissolution pore, DB5-12; f. fine crystalline dolomite, secondary cement filled in the dissolution pore, DB5-10).

μm in diameter (Fig. 2b and c). Some bioclasts contained cavities but is relatively low. Dolomite crystals in RD1 are small, and mainly distributed within several microns to dozens of microns (Fig. 2d). There were few secondary cements filled in the mold pores, and the crystals were small (Fig. 2d). The particles in RD2 were coarse and generally distributed within 100–200 μm, and dolomite enlargement was observed (Fig. 2e–f). Some fractures and dissolved pores were developed. The fractures were mostly filled with secondary dolomite cement, and the cement crystal was larger than the matrix at up to hundreds of microns.

4.2. Major and trace elements composition

The result of element analysis is shown in Table 1. The average content of Ca was 36.50%, and that of Mg was 15.79%. The contents of Fe and Mn were relatively low, with Fe less than 0.50%, Mn less than 0.02%, and Al less than 0.5%.

The content of Sr ranges from 61 to 235 ppm, with an average of 126 ppm. The contents of Th, Sc, and Zr were low. The contents of Th and Sc were basically lower than 1.0 ppm, with averages of 0.43 and 0.76 ppm, while the content of Zr was relatively high, with an average of 2.32 ppm.

4.3. Rare earth elements composition

REEs can generally be well preserved over a long geological history period, and the characteristics of REEs and Y can be used to analyze the original sedimentary environment. The anomalies of REEs are calculated using the following formula:

$La/Yb(\mathrm{PAAS}) = La^*/Yb^*$; $\delta Ce = Ce^*/\sqrt{La^* \times Pr^*}$; $\delta Eu = Eu^*/\sqrt{Sm^* \times Gd^*}$; $\sum REE = SUM(La, Ce, Pr, Nd, Sm, Eu, Gd, Tb, Dy, Ho, Er, Tm, Yb, Lu)$; *: value is standardized with Post-Archean Australian Shale (PAAS).

As shown in Table 2, the REE + Y patterns were generally of a flat shale type (Fig. 3). The total amount of REEs in the samples was low, generally lower than 12 ppm, with an average of 11.58 ppm. There was a certain degree of light REE enrichment, overall showing a certain degree of negative Ce anomaly and no anomaly of Eu. The Y/Ho ratio was generally greater than 30, with an average of 32.44.

4.4. Isotopic characteristics

Seven samples were selected for the determination of C and O isotopes (Table 3). The $\delta^{13}C$ value was distributed between −0.1 and + 1.0‰, and $\delta^{18}O$ was distributed between −9.2 and −2.4‰. C isotopes are distributed in the range of normal seawater; however, O isotopes show a certain degree of negative bias, and C and O isotopes show a certain correlation (Fig. 4).

The $^{87}Sr/^{86}Sr$ ratio is generally used to determine the change in the global sea level because of its long-term stability in geological history. Five samples were selected for Sr isotope tests, and the results fluctuated between 0.7089 and 0.7095, with an average of 0.708939 (Table 3), which was similar to the Sr isotopes value of global seawater during the Middle Ordovician (0.7084–0.7090, Vollstaedt et al., 2014; Jiang et al., 2019).

5. Discussion

5.1. Sample contamination assessment

5.1.1. Evaluation of detrital contamination

The REE composition of carbonate rocks is easily affected by non-carbonate components, such as detrital inputs, whether in the early or late diagenesis (Banner et al., 1988; Ren et al., 2019; Prasanta and Sarada, 2021). To prevent these impurities from changing the results, it was necessary to assess the degree of detrital contamination in our samples.

The REE + Y distribution of carbonate samples represents the original sedimentary environment, which is established when the REE content is low. The following parameters can be used to evaluate whether the samples were polluted by detrital components. ∑REEs is less than 12 ppm, Y/Ho is greater than 26, Ti is less than 0.5%, Al is less than 1%, Th, Zr, and Hf are less than 20 ppm, these parameters indicate samples free of terrigenous debris (Bolhar et al., 2004; Sarangi et al., 2017; Jiu et al., 2021; Prasanta and Sarada, 2021). There will not be much Sc in the chemical

Table 2
Rare earth elements and Y element composition.

Sample	Depth, m	Rare earth elements composition, ppm									
		La	Ce	Pr	Nd	Sm	Eu	Gd	Tb	Dy	Ho
DB18-4	4009.50	2.70	5.23	0.62	2.64	0.72	0.17	0.77	0.12	0.69	0.14
DB18-5	4008.52	2.00	3.91	0.47	2.00	0.46	0.10	0.45	0.07	0.44	0.08
DB5-10	3834.7	1.18	2.21	0.25	0.99	0.20	0.05	0.22	0.04	0.21	0.04
DB5-12	3830.85	1.03	1.89	0.22	0.97	0.21	0.05	0.21	0.04	0.23	0.04
DB8-8	4269.28	1.48	2.89	0.33	1.31	0.24	0.05	0.26	0.03	0.16	0.03
DB8-11	4270.49	1.82	3.41	0.39	1.69	0.36	0.08	0.35	0.07	0.38	0.08
DB10-4	3904.40	2.13	4.15	0.49	2.23	0.64	0.18	0.77	0.11	0.58	0.12

Sample	Depth, m	Rare earth elements composition, ppm				Y, ppm	∑REE	δCe	δEu	Y/Ho
		Er	Tm	Yb	Lu					
DB18-4	4009.50	0.35	0.05	0.32	0.05	4.21	18.76	0.88	0.99	30.07
DB18-5	4008.52	0.21	0.03	0.18	0.02	2.54	12.97	0.87	0.95	32.15
DB5-10	3834.7	0.12	0.02	0.12	0.02	1.29	6.94	0.89	0.94	34.86
DB5-12	3830.85	0.13	0.02	0.10	0.02	1.28	6.42	0.87	1.01	33.68
DB8-8	4269.28	0.11	0.02	0.10	0.01	0.94	7.97	0.90	0.94	27.65
DB8-11	4270.49	0.24	0.04	0.21	0.03	2.65	11.79	0.88	0.92	33.13
DB10-4	3904.40	0.37	0.05	0.29	0.04	4.09	16.23	0.88	1.14	35.57

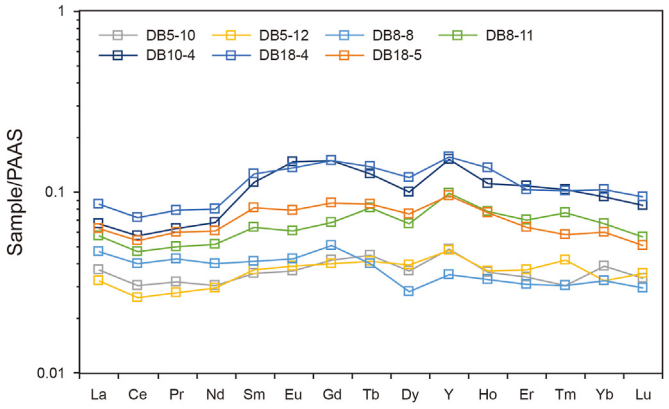

Fig. 3. REE + Y characteristics in the Dingbei area. Standardization is based on the REE composition of PAAS. Since the atomic radius of Y is similar to that of Dy and Ho, Y was placed between Dy and Ho.

deposition process compared with the clastic rock. If the Sc content is greater than 2 ppm, the sample might be strongly contaminated. In this study, the average ∑REEs content was 11.58 ppm, Ti was less than 0.02%, Al was less than 0.5%, Y/Ho was greater than 27, Zr, Hf, and Th were less than 20 ppm and Sc was less than 2 ppm (Table 2), the overall sample data were within the specified "no pollution" range. Therefore, REE + Y contents can represent the original sedimentary paleoenvironment.

The Y/Ho parameter of terrigenous clasts remains ~26. The characteristic ratio of detrital components would cover the original seawater, although the amount of terrigenous detritus is small; a good correlation between Y/Ho–δCe and Zr can be observed; and Al, Th, Sc, and Zr are enriched in detrital components. When a certain number of detrital components are observed, an obvious negative correlation between Al, Th, Zr, Sc, and Y/Ho exists (Duda et al., 2014; Sarangi et al., 2017); however, this good correlation has not been presented in the scatter diagram (Fig. 5a–d). Furthermore, δCe has a poor negative correlation with Al, Th, and Zr (Fig. 5e–g), but no correlation with Sc (Fig. 5h). The scatter diagram of Y/Ho and Nd concentrations can characterize the changing trend affected by pure chemical deposition and detritus. As shown below, the samples fell into the pure chemical deposition area (Fig. 6). Similarly, the content of Rb in seawater is very low, generally less than 30 ppm (Krabbenhöft et al., 2010), but it is rich in feldspar, mica and clay minerals. The Rb content of the samples from the study area was less than 5 ppm (Table 1). In conclusion, the samples from the Dingbei area indicated a chemical deposition process, and the possibility of detrital components affecting REEs distribution can be ruled out.

The influence of oxides and sulfides cannot be ignored in the process of carbonate deposition. Cu and Ni were selected as representatives to monitor oxides, and Sc and Pb were used to characterize the effects of sulfides (Bolhar and Van Kranendonk, 2007; Prasanta and Sarada, 2021). The lower contents of Cu and Ni and their weak or lack of correlation with Y/Ho indicated that oxides had no effect on the samples (figure not provided). Furthermore, as shown in Fig. 5d and i, there were no correlation between Sc or Pb and Y/Ho, indicating that no sulfide influences were possible.

The retention time of Sr isotopes in seawater (about 10^6 a) far exceeds the mixing time (approximately 10^3 a), and it will not be fractionated under the influence of temperature, pressure, and microorganisms. The $^{87}Sr/^{86}Sr$ ratio in the study area is within the

Table 3
C/O and Sr isotope composition.

Sample	Depth, m	C/O isotope composition, ‰			Sr isotope composition	
		$\delta^{13}C_{V\text{-}PDB}$	$\delta^{18}O_{V\text{-}PDB}$	$\delta^{18}O_{V\text{-}SMOW}$	$^{87}Sr/^{86}Sr$	Standard Error
DB18-4	4009.50	+0.6	−3.3	27.0	0.709512	0.000018
DB18-5	4008.52	+1.0	−2.4	27.9	/	/
DB5-10	3834.70	+0.9	−4.9	25.5	0.709043	0.000021
DB5-11	3832.50	+0.9	−4.9	25.4	/	/
DB5-12	3830.85	+0.9	−5.4	25.0	0.709278	0.000022
DB8-11	4270.49	+0.2	−8.3	22.2	0.708939	0.000016
DB10-4	3904.40	−0.1	−9.2	21.3	0.708974	0.000018

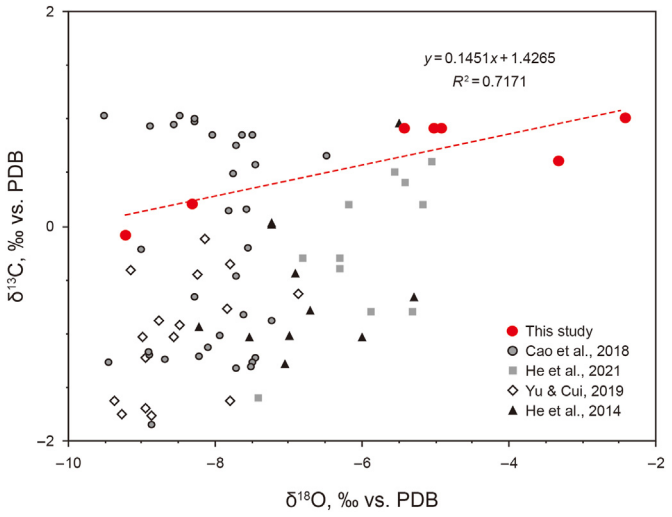

Fig. 4. C and O isotope distribution in Ma_5 Fm. from various published sources (The collected isotopic data of carbonate matrix do not show correlation, but the C and O isotopes in the study area showed a certain positive correlation).

range of the Middle Ordovician seawater (Table 3) (Henderson et al., 2018). If affected by terrigenous debris, this $^{87}Sr/^{86}Sr$ ratio should be much higher than that of seawater in the same period.

5.1.2. Evaluation of metamorphic and diagenetic alterations

Fe and Mn in carbonate rocks are very sensitive to metamorphism and post diagenesis, and they generally show enrichment (Sarkar et al., 2003). Although REEs can generally maintain their characteristics under metamorphism, heavy REEs loss, Ce loss, and Eu enrichment usually occur under the conditions of high temperatures and water–rock ratio. Therefore, a negative correlation will exist between Fe, Mn, δCe, and ∑REEs, however, this correlation was not found in this study (Fig. 7). The ratio of La/Yb(PAAS) in the study area was generally less than 1.0 (expect DB8-8 = 1.45), indicating the elements' components represented the original seawater and that the influence of metamorphism was excluded (Ren et al., 2019).

There are Sabkha and brine-reflex dolomitization models in the study area (e.g., Zhang et al., 2017). The dolomite associated with gypsum was developed in the Sabkha dolomitization model, and the crystal size is generally small (Allan and Wiggins, 1993), about

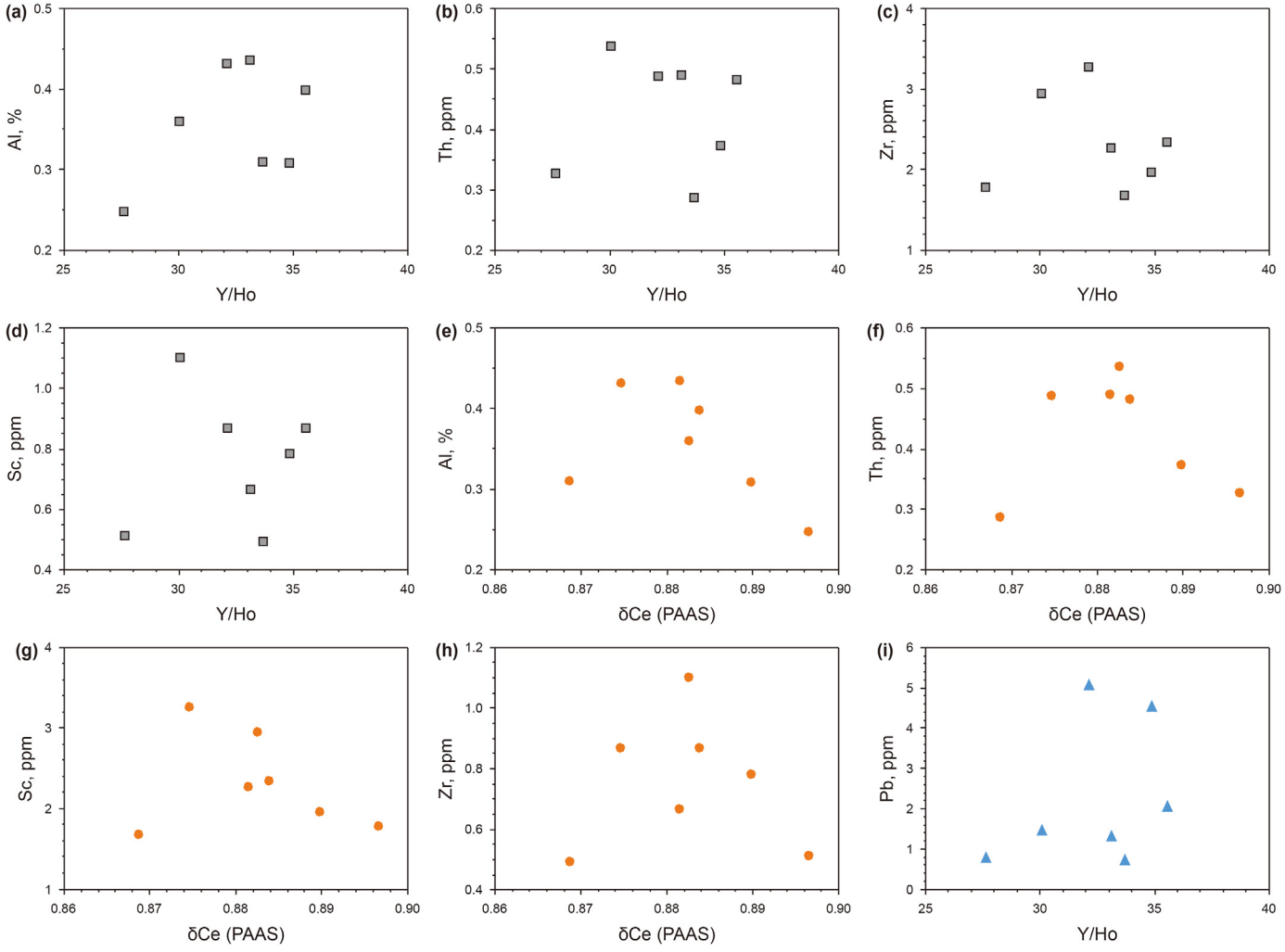

Fig. 5. Cross-plots of geochemical data of carbonates for assessing detrital contamination in the Dingbei area.

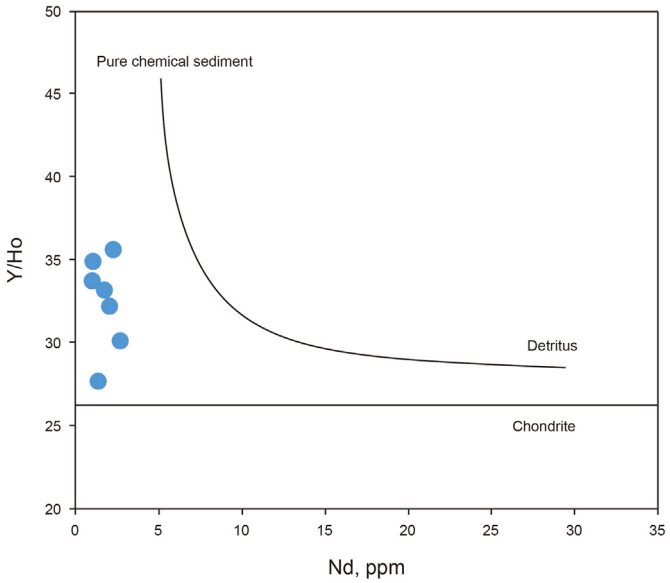

Fig. 6. Y/Ho vs. Nd concentration for the Dingbei carbonates. A low concentration of Nd indicates that samples are pure chemical precipitates without detrital contaminations (detritus and chondrite trends are adopted from Viehmann et al., 2015).

tens of microns (Fig. 2b, d). And the brine-reflex dolomitization led to the increased size of crystals, brighter enlarged edges than cores can be observed, and the crystal is generally several hundred microns (Fig. 2c, e-f). However, neither dolomitization nor the late diagenetic alteration process has little or no influence on the REE + Y distribution (i.e., Banner et al., 1988; Prasanta and Sarada, 2021). When dolomite is affected by early meteoric water, the Mn content is generally distributed in the range of 100–600 ppm, and Fe content is widely distributed in the range of 2000–10000 ppm in the Ordos Basin (Li, 2020), which is completely consistent with the data obtained (Table 1). It is generally believed that $\delta^{18}O$ will show a low isotopic composition after experiencing the influence of meteoric water, but when $\delta^{18}O$ is lower than −10.0‰, carbonate samples are generally considered to have been affected by hydrothermal fluids (He et al., 2014). The $\delta^{18}O$ in the study area was generally low but was greater than −10.0‰. The weak correlation between the C and O isotopes (Fig. 4), combined with the elements' information of Fe and Mn, all indicate the dolomite in the study had experienced early meteoric water dissolution. However as shown in Fig. 8a and b, there was no correlation between δCe and Dy/Sm (PAAS) and a weak negative correlation between δEu and Pr/Sm (PAAS) indicated that Eu was not involved in late diagenesis (Konhauser et al., 2017), which was consistent with the conclusion that there was no Eu anomaly in the samples we obtained. In the diagenetic process, carbonate rocks will show the enrichment of Mn and Fe and the loss of Sr (Huang et al., 2006). Therefore, if affected by diagenesis, there should be an obvious positive correlation between Fe and Mn, however, there was no correlation between Fe and Mn in the samples (Fig. 8c). In conclusion, diagenesis had an extremely weak impact on the samples.

5.2. Paleoenvironment restoration

In light of the little evidence for later diagenetic alteration, marine carbonate rocks may well inherit the REE distribution from the original marine environment (i.e., Lottermoser, 1992; Webb and Kamber, 2000; Nothdurft et al., 2004).

5.2.1. Characteristics of paleoredox conditions

The ratios of trace elements V/Cr, U/Th, Ni/Co, and V/(V + Ni) are widely used to analyze the evolution of paleoredox conditions (Hatch and Leventhal, 1992; Jones and Manning, 1994; Prasanta and Sarada, 2021). A Ni/Co ratio <5 develops in oxic conditions, between 5 and 7 develops in dysoxic conditions, and that >7 develops in suboxic to anoxic conditions, whereas V/Cr is bounded by 2 and 4.25, representing oxic, dysoxic, and suboxic–anoxic conditions, respectively (Jones and Manning, 1994). An anoxic environment in sedimentary strata is rich in U, so the Th/U ratio is low, ~2 is generally found in marine anoxic conditions, and that >2 is found in oxic environments, moreover, the higher the ratio, the higher the oxic degree (Rimmer, 2004). The above thresholds were obtained from a large number of clastic rock studies. In carbonate rocks, owing to the relatively low content of trace elements, the thresholds should be modified accordingly, but the overall trend indicates that an oxic or anoxic environment is certain. Prasanta and Sarada (2021) believed that V/(V + Ni) ratios of 0.3 and 0.5 in carbonate rocks and U/Th ratios of 0.2 and 0.5 are the boundaries of oxic, dysoxic, and suboxic conditions. As shown in Fig. 9, the obtained trace element ratios were in the suboxic–anoxic range.

Ce is sensitive to the redox conditions of a diagenetic environment. Under oxic conditions, Ce^{3+} tends to change its valence state to form tetravalent ions in sediments, resulting in an obvious negative Ce anomaly in diagenetic fluid (Sverjensky, 1984; Frimmel, 2009), hence, it will show a positive Ce anomaly in minerals. However, the samples obviously showed a negative Ce anomaly, with an average δCe of 0.88, which also proved that the carbonate rocks in the Dingbei area were precipitated in suboxic–anoxic conditions.

5.2.2. Paleotemperature recovery

The Sr/Ba ratio is extremely sensitive to the evaporation environment and can be used to reflect the change in temperature in the original sedimentary environment (Jiu et al., 2021). There

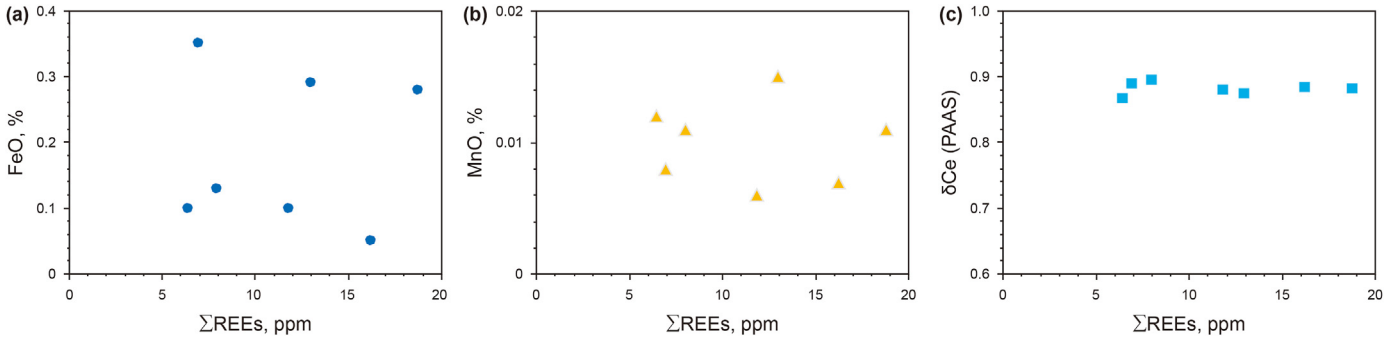

Fig. 7. Cross-plots of geochemical data of carbonates for assessing metamorphism in the Dingbei area. There is no correlation between the metamorphism proxy and the content of ∑REEs, indicating that the samples' geochemical characteristics were not affected by metamorphism.

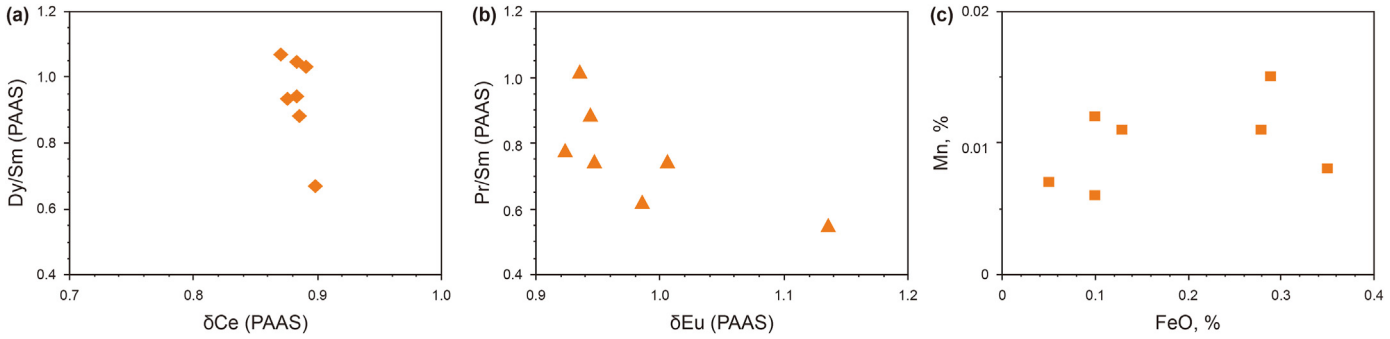

Fig. 8. Cross-plots of geochemical data of carbonates for assessing diagenesis in the Dingbei area.

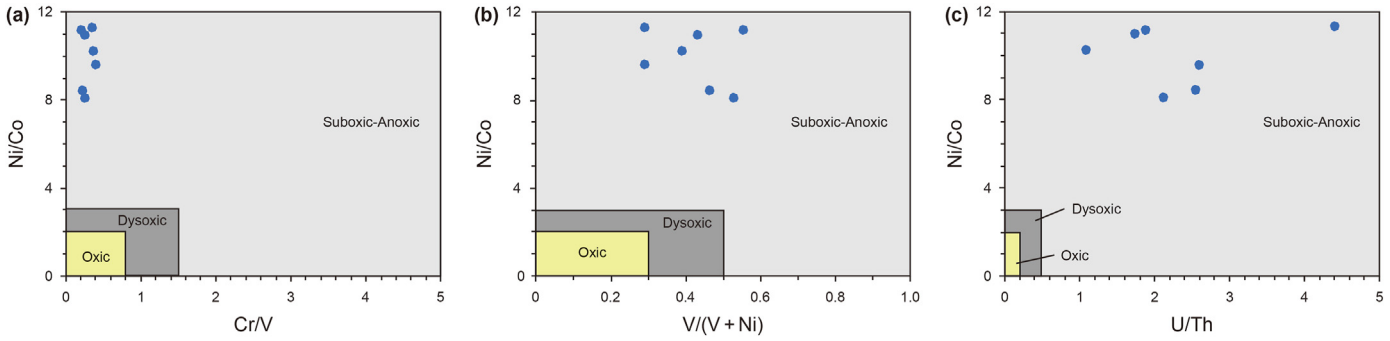

Fig. 9. Analysis diagram of paleoredox conditions of carbonate rock. The data of this study show that the paleoredox of Ma5 Fm. is suboxic-anoxic (plate from Prasanta and Sarada, 2021).

seems to be some relationship between Sr and Ba (Fig. 10a), and the obtained Sr/Ba ratio was high, up to 18.08, indicating that the original sedimentary environment was arid, which was consistent with the previous conclusion that the dolomitization mode in Ma5 Fm. in other areas of the Ordos Basin, like the Daniudi gas field, was the Sabkha (e.g., Zhang et al., 2017; He et al., 2020). This also provided geochemical evidence for an original sedimentary source of much gypsum (later dissolved into mold pores) in the samples (Fig. 2d). It is worth noting that there was a certain positive correlation between Sr/Ba and ΣREEs (Fig. 10b), which may indicate that there was a certain coupling relationship between the preservation of REEs and the production of evaporated minerals with the increase in the paleotemperature. This may also lead to the increase in the FeO/MnO ratio with the increase in the ΣREEs (Fig. 10c). Conversely, the correlation between the Sr and CaO content was more obvious in the study area (Fig. 10d). The Sr/Ca ratio is very sensitive to weathering and evaporation (Fairchild et al., 2000), but the change in this ratio in the study area was minimal, which proved the samples were not affected by strong weathering in the later stage, and the arid environment in this area was relatively stable. Therefore, it was possible to develop thick dolomites in an evaporation environment in Ma5 Fm. of the Ordos Basin.

The $\delta^{18}O$ value of carbonate rocks is widely used as a proxy to reconstruct paleotemperature during the sedimentary period (e.g., Vasconcelos et al., 2005; Ren et al., 2019), and the calculated temperature is generally that of carbonate precipitation fluid. The $\delta^{18}O$ of the Middle Ordovician ancient seawater is approximately from −6.6 to −4.0‰, and −5.3‰ is selected as the average $\delta^{18}O$ of seawater proxy (Li, 2020; Albanesi et al., 2020). The average $\delta^{18}O$ obtained was −5.47‰. We used the formula below (Land, 1983) to calculate the temperature:

$$1000 \ln a_{\text{dolomite-seawater}} = 3.2 \times 10^6 T^{-2} - 3.3$$

where a is the O isotope fractionation coefficient between dolomite and seawater, and T is the thermodynamic temperature.

The calculated results showed the average temperature during dolomite deposition was 29 °C. Considering that the sample is affected by early meteoric water to a certain extent and analytical (~3 °C range) uncertainties, the real paleotemperature should be higher, and it is still similar to the seawater temperature at that time (about 30 °C, Trotter et al., 2008).

5.2.3. Paleosalinity reconstruction

Na content was used to reflect the salinity of the fluid (Marriott et al., 2004; Geerken et al., 2018). The Na content of the carbonate samples ranged from 100 to 880 ppm, with an average of 364 ppm (Table 1). According to a previous elemental analysis of pure dolomites deposited in a limited lagoon of the Longwangmiao Formation in the Sichuan Basin, the Na content was only 218 ppm (Wang et al., 2021), indicating that the salinity in the study area during the Dw2-Dw3 was significantly higher than that in the limited environment. In particular, the discovery of a large number of gypsum rocks and gypsum mold pores further confirms the development of higher paleosalinity (Fig. 2d) (e.g., Zhang et al., 2016).

As discussed above, the sea temperature was high and the sea level was at the cycle stage of regression. The dolomitization fluid comes from seawater, with high seawater temperature and arid environment, these characteristics are completely consistent with the Sabkha dolomitization. Therefore, it is reasonable to believe that the dolomitization model in the Dingbei area is consistent with that in other areas of the Ordos Basin, which is the Sabkha model,

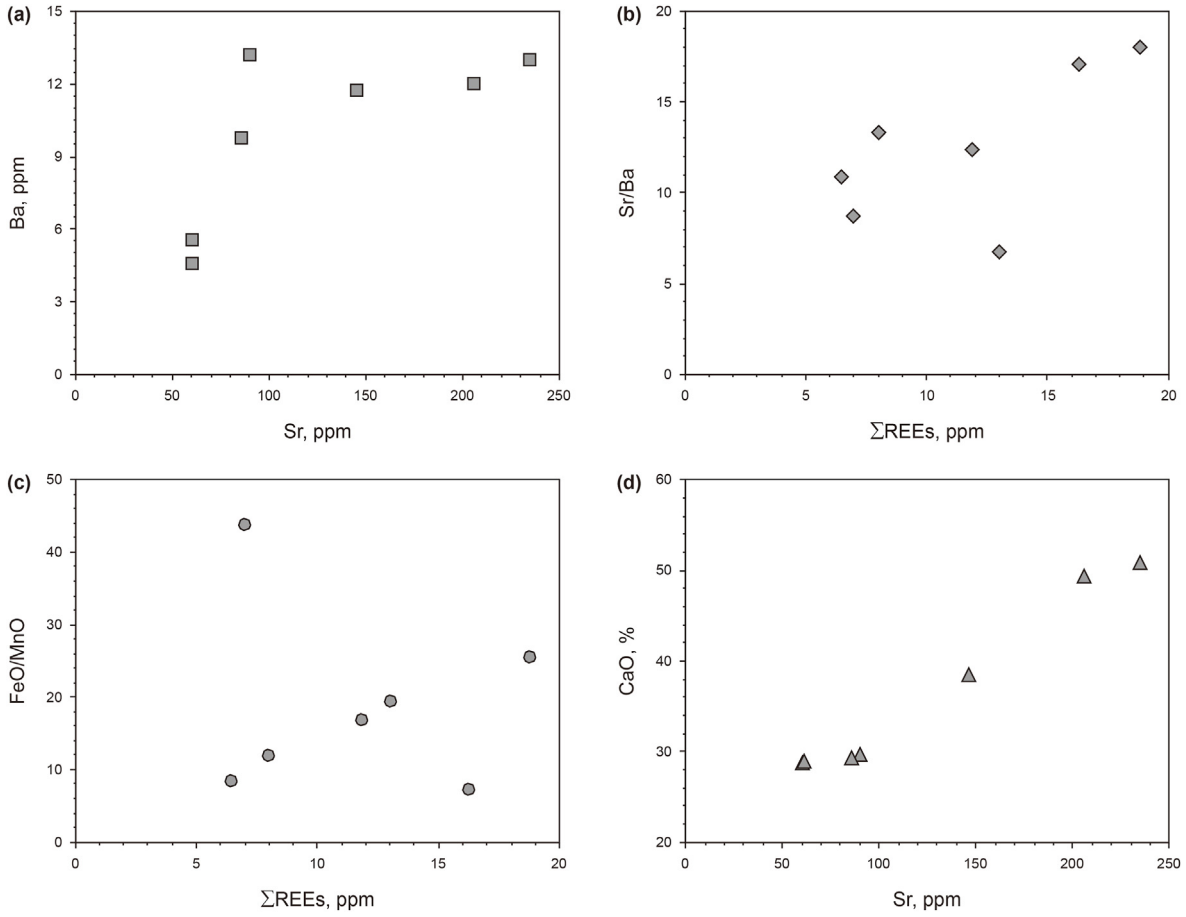

Fig. 10. Cross-plots of geochemical data of carbonates showing an evaporation environment of Ma5 Fm. in the Dingbei area.

furthermore, the sedimentary environment of the study area should be limited tidal flat. An increase in the evaporation intensity led to a gradual increase in seawater salinity. High seawater salinity is more conducive to the Sabkha dolomitization and gypsum precipitation (e.g., Warren, 2000; Allan and Wiggins, 1993), which may provide a material basis for the subsequent dissolution of meteoric water, to form a high-quality reservoir (Xiong et al., 2016).

5.3. Response of isotope carbon excursion to paleoenvironment

The $\delta^{13}C$ excursion is influenced by many factors. A positive excursion may be affected by an increase in marine reservoir productivity (Kump et al., 1999) and the weathering intensity of the carbonate platform (Hu et al., 2017). The fundamental principle is a large amount of light carbon was consumed in seawater dissolved inorganic carbon (DIC) reservoir (Saltzman and Edwards, 2017). This is consistent with our experimental results, the C isotope excursion may be caused by much plankton in this biological explosion carrying out photosynthesis (e.g., Schmitz et al., 2010; Chen, 2019; Danelian and Monnet, 2021).

The seawater paleotemperature in the Dw2-Dw3 is high, about 29 °C. Compared with the seawater temperature in the Early Ordovician (up to 45 °C, Trotter et al., 2008; Albanesi et al., 2020), it shows a gradual downward trend, which is consistent with the previous Ordovician temperature change trend (e.g., Henderson et al., 2018; Chen, 2019). During this process, the temperature gradually became appropriate for organisms, resulting in multiple biological blooms (Chen, 2019). The seawater temperature of Dw2-Dw3 is more suitable for organisms, leading to a large-scale biological explosion, which eventually presents a C isotope excursion (MDICE) around the world (Albanesi et al., 2020). And the peak of the excursion occurs well within the *Eoplacognathus suecicus* Zone (Saltzman and Edwards, 2017; Bergström et al., 2009, 2020).

The light carbon isotope (^{12}C) preferentially enters the photosynthesis products, enriching ^{13}C in the DIC reservoir (Hayes et al., 1999), and resulting in the increase in buried organic matter and shape decrease in CO_2 in the atmosphere. The MDICE may be related to the biological explosion caused by the temperature falling to an environment suitable for biological survival. However, the Ordovician marine redox interface fluctuated sharply and suboxic–anoxic conditions were widespread (Fig. 9) (Marenco et al., 2013; D'Arcy et al., 2017), which is not consistent with the results of biological explosion. This is possibly due to the extremely high concentration of atmospheric CO_2 (about 14–18 times that of the present time) reducing the temperature gradient from the equator to the poles, which slowed down the global thermohaline circulation, and finally made it difficult for surface dissolved oxygen to migrate downward (Marenco et al., 2013; Kah et al., 2016; D'Arcy et al., 2017). High paleotemperature (might more than 29 °C) slowed the oxygen cycle in water volume, and the biological prosperity (Fig. 2a) promoted further consumption of seawater dissolved oxygen, leading to reducing conditions (Pan et al., 2020).

5.4. Impact of paleoenvironment on natural gas exploration

High seawater paleotemperature and paleosalinity not only

provide conditions for dolomitization but also make large-scale gypsum precipitation possible. Gypsum rock is more prone to dissolution compared with dolomite. Under the influence of meteoric water, many gypsum rocks in the sedimentary period dissolved and produced a large number of secondary dissolution pores. Later, affected by weathering, the fillings did not block the dissolution pores during burial, which guaranteed the formation of high-quality reservoirs (He et al., 2013; Qi and Guo, 2017; Zhang et al., 2017; Jiu et al., 2021). The biogenic framework pores are also a reservoir space that cannot be ignored, although these pores in L1 were basically filled by later recrystallization; furthermore, if there was oil and/or gas filling in the early stage, it inhibited the progress of recrystallization and preserved the pores.

Even under the influence of meteoric water, when a certain thickness is developed, the layered gypsum rock will not be completely dissolved and can be used as a direct cover or floor to protect the reservoir from damage in the later stage. Because of its own toughness, it can protect the reservoir to a certain extent, even after a strong tectonic movement.

Meanwhile, during the MDICE event, a large number of plankton propagated under the seawater surface, and the biological yield and buried organic matter increased, resulting in further anoxia in the seawater column, which in turn promoted the burial and preservation of organic matter, resulted in the rapid increase in TOC (Pan et al., 2020). The TOC of loads of argillaceous dolomites and dolomitic mudstones could exceed 1%, even some reached 5%, which could be used as effective source rocks to supply hydrocarbon to nearby high-quality reservoirs (i.e., Tu et al., 2016; Li et al., 2017; Xu et al., 2021) In the subsequent burial process, after reaching a certain temperature, the organic content could generate hydrocarbons in large numbers, which could be used as a supplement to the main source rock to provide natural gas.

6. Conclusions

Based on the analyses of elements, isotopic compositions, and lithological characteristics, the Ma5 Fm. in the Dingbei area mainly developed intraclast biological micritic limestone, silty dolomite, and fine crystalline dolomite. The $\delta^{13}C$ of the carbonate samples showed significant positive excursion, corresponding to the MDICE event. The paleotemperature during the deposition period was about 29 °C, furthermore, the seawater salinity was high, corresponding to suboxic–anoxic conditions.

Due to the prosperity of plankton, photosynthesis under the seawater surface and significantly suboxic–anoxic conditions, the burial and preservation of organic matter were promoted. The Middle Ordovician carbonate rock can be used as a supplement to the main source rock to provide natural gas. Affected by the paleoenvironment, the development of gypsum rock strata provided a material basis for early meteoric water dissolution, and guaranteed the formation of high-quality reservoirs in Ma5 Fm. At the same time, the residual gypsum played a sealing role to a certain extent to protect the reservoir from damage. A good source-reservoir-cap configuration provided the conditions for the preservation of reservoirs.

Declaration of competing interest

The authors declare that they have no known competing financial interests or personal relationships that could have appeared to influence the work reported in this paper.

Acknowledgements

This study was financially supported by the National Natural Science Foundation of China (U19B6003), Frontier Project of Chinese Academy of Sciences (XDA14010201), and National Key Natural Science Foundation of China (91755211).

References

Albanesi, G.L., Bergström, S.M., Schmitz, B., et al., 2013. Darriwilian (middle ordovician) $\delta^{13}C_{carb}$ chemostratigraphy in the precordillera of Argentina: documentation of the middle darriwilian isotope carbon excursion (MDICE) and its use for intercontinental correlation. Palaeogeogr. Palaeoclimatol. Palaeoecol. 389, 48–63. https://doi.org/10.1016/j.palaeo.2013.02.028.

Albanesi, G.L., Barnes, C.R., Trotter, J.A., et al., 2020. Comparative Lower-Middle Ordovician conodont oxygen isotope palaeothermometry of the Argentine Precordillera and Laurentian margins. Palaeogeogr. Palaeoclimatol. Palaeoecol. 549, 1–13. https://doi.org/10.1016/j.palaeo.2019.03.016.

Allan, J.R., Wiggins, W.D., 1993. Dolomite Reservoirs: Geochemical Techniques for Evaluating Origin and Distribution. American Association of Petroleum Geologists.

An, T., Zheng, Z., 1990. The Conodonts of the Marginal Areas Around the Ordos Basin North China. Science Press, Beijing, pp. 104–115 (in Chinese).

Ainsaar, L., Meidla, T., Tinn, O., 2004. Middle and Upper Ordovician stable isotope stratigraphy across facies belts in the East Baltic. In: Hints, O., Ainsaar, L. (Eds.), WOGOGOB-2004 Conference Materials. Tartu University Press, Tartu, pp. 11–12.

Banner, J.L., Hanson, C.N., Meyers, W.J., 1988. Rare-earth element and Nd isotopic variations in regionally extensive dolomites from the Burlington-Keokuk Formation (Mississippian); implications for REE mobility during carbonate diagenesis. J. Sediment. Res. 58 (3), 415–432. https://doi.org/10.1306/212F8DAA-2B24-11D7-8648000102C1865D.

Bergström, S.M., Chen, X., Gutiérrez-Marco, J.C., et al., 2009. The new chronostratigraphic classification of the Ordovician System and its relations to major regional series and stages and to $\delta^{13}C$ chemostratigraphy. Lethaia 42 (1), 97–107. https://doi.org/10.1111/j.1502-3931.2008.00136.x.

Bergström, S.M., Eriksson, M., Ahlberg, P., 2020. Ordovician $\delta^{13}C$ Chemostratigraphy: A Global Review of Major Excursions and Their Ties to Graptolite and Conodont Biostratigraphy. Science Direct. Elsevier, pp. 319–351.

Bolhar, R., Kamber, B.S., Moorbath, S., et al., 2004. Characterisation of early Archaean chemical sediments by trace element signatures. Earth Planet Sci. Lett. 222, 43–60. https://doi.org/10.1016/j.epsl.2004.02.016.

Bolhar, R., Van Kranendonk, M.J., 2007. A non-marine depositional setting for the northern Fortescue Group, Pilbara Craton, inferred from trace element geochemistry of stromatolitic carbonates. Precambrian Res. 155, 229–250. https://doi.org/10.1016/j.precamres.2007.02.002.

Calner, M., Lehnert, O., Wu, R., et al., 2014. $\delta^{13}C$ chemostratigraphy in the lower-middle ordovician succession of Öland (Sweden) and the global significance of the MDICE. Gff 136 (1), 48–54. https://doi.org/10.1080/11035897.2014.901409.

Cao, H., Shang, T., Wu, H., et al., 2018. Characteristic of carbon and oxygen isotopes of carbonate rocks in Majiagou Formation and their implication, southeastern Ordos Basin. J. NW Univ. 48 (4), 578–586. https://doi.org/10.16152/j.cnki.xdxbzr.2018-04-013 (in Chinese).

Chen, K.F., 2019. The Ocean Chemistry Changes Associated with the GOBE in Ordovician. Thesis, University of Science and Technology of China, pp. 1–40 (in Chinese).

Chen, L., Yi, H.S., Tsai, L., et al., 2013. Jurassic black shales facies from Qiangtang basin (northern Tibet): rare earth and trace elements for paleoceanographic implications. Acta Geol. Sin. 87 (2), 540–554. https://doi.org/10.1111/1755-6724.12067.

D'Arcy, J., Gilleaudeau, G.J., Peralta, S., et al., 2017. Redox fluctuations in the early ordovician oceans: an insight from chromium stable isotopes. Chem. Geol. 448, 1–12. https://doi.org/10.1016/j.chemgeo.2016.10.012.

Danelian, T., Monnet, C., 2021. Early paleozoic radiolarian plankton diversity and the Great ordovician biodiversification event. Earth Sci. Rev. 218, 103672. https://doi.org/10.1016/j.earscirev.2021.103672.

Dixon, D., Jenkins, I., Moody, R., 2001. Atlas of Life on Earth: the Earth, its Landscape and Life Forms. Barnes and Noble Books, pp. 1–368.

Duda, P., Blumenberg, M., Thiel, V., et al., 2014. Geobiology of a palaeoecosystem with ediacara-type fossils: the shibantan member (dengying formation, South China). Precambrian Res. 255, 48–62. https://doi.org/10.1016/j.precamres.2014.09.012.

Fairchild, I.J., Borsato, A., Tooth, A.F., et al., 2000. Controls on trace element (Sr–Mg) compositions of carbonate cave waters: implications for speleothem climatic records. Chem. Geol. 166, 255–269. https://doi.org/10.1016/S0009-2541(99)00216-8.

Frimmel, H., 2009. Trace element distribution in Neoproterozoic carbonates as Paleoenvironmental indicator. Chem. Geol. 258, 338–353. https://doi.org/10.1016/j.chemgeo.2008.10.033.

Fu, S.Y., Zhang, C.G., Chen, H.D., et al., 2019. Characteristics, formation and evolution of pre-salt dolomite reservoirs in the fifth member of the Ordovician Majiagou Formation, mid-east Ordos Basin, NW China. Petrol. Explor. Dev. 46 (6), 1087–1098. https://doi.org/10.1016/S1876-3804(19)60270-3.

Folk, R.L., 1962. Spectral subdivision of limestone type. In: Ham, W.E. (Ed.), Classification of Carbonate Rocks: A Symposium. AAPG, Tulsa, OK, pp. 62–84.

Goldman, D., Sadler, P.M., Leslie, S.A., et al., 2020. The Ordovician Period. In:

Gradstein, F.M., Ogg, J.G., Schmitz, M.D., Ogg, G.M. (Eds.), Chapter 20. Geologic Time Scale. Elsevier. https://doi.org/10.1016/B978-0-12-824360-2.00020-6.
Geerken, E., Nooijer, L.J., Dijk, I.V., et al., 2018. Impact of salinity on element incorporation in two benthic foraminiferal species with contrasting magnesium contents. Biogeosciences 15, 2205–2218. https://doi.org/10.5194/bg-15-2205-2018.
Haq, B.U., Schutter, S.R., 2008. A chronology of Paleozoic sea-level changes. Science 355 (5898), 64–68. https://www.jstor.org/stable/20144943.
Hatch, J.R., Leventhal, J.S., 1992. Relationship between inferred redox potential of the depositional environment and geochemistry of the upper Pennsylvanian (Missourian) Stark shale member of the dennis limestone, Wabaunsee county, USA. Chem. Geol. 99, 65–82. https://doi.org/10.1016/0009-2541(92)90031-Y.
Hayes, J.M., Strauss, H., Kaufman, A.J., 1999. The abundance of ^{13}C in marine organic matter and isotopic fractionation in the global biogeochemical cycle of carbon during the past 800 Ma. Chem. Geol. 161, 103–125. https://doi.org/10.1016/S0009-2541(99)00083-2.
He, J., Fang, S., Hou, F., et al., 2013. Vertical zonation of weathered crust ancient karst and the reservoir evaluation and prediction—a case study of M_5^5–M_5^1 sub–members of Majiagou Formation in gas fields, central Ordos Basin, NW China. Petrol. Explor. Dev. 40 (5), 534–542. https://doi.org/10.1016/S1876-3804(13)60075-0.
He, M., Huang, W., Jiu, B., 2021. Origin and evolution of gypsum dolomite as a favorable reservoir in the Ordos basin, China. Earth Sci. Front. 28 (4), 327–336. https://doi.org/10.13745/j.esf.sf.2020.5.6 (in Chinese).
He, X., Shou, J., Shen, A., et al., 2014. Geochemical characteristics and origin of dolomite: a case study from the middle assemblage of ordovician Majiagou Formation member 5 of the west of Jingbian gas field, Ordos Basin, North China. Petrol. Explor. Dev. 41 (3), 417–427. https://doi.org/10.1016/S1876-3804(14)60048-3.
He, Z., Ma, Y., Zhang, J., et al., 2020. Distribution, genetic mechanism and control factors of dolomite and dolomite reservoirs in China. Oil Gas Geol. 41 (1), 1–14. https://doi.org/10.11743/ogg20200101 (in Chinese).
Henderson, M.A., Serra, F., Feltes, N.A., et al., 2018. Paired isotope records of carbonate and organic matter from the middle ordovician of Argentina: intrabasinal variation and effects of the marine chemocline. Palaeogeogr. Palaeoclimatol. Palaeoecol. 490, 107–130. https://doi.org/10.1016/j.palaeo.2017.10.018.
Hu, D., Zhang, X., Zhou, L., et al., 2017. $^{87}Sr/^{86}Sr$ evidence from the epeiric Martin Ridge Basin for enhanced carbonate weathering during the Hirnantian. Sci. Rep-UK 7, 11348. https://doi.org/10.1038/s41598-017-11619-w.
Huang, S.J., Qing, H.R., Pei, C.R., et al., 2006. Strontium concentration, isotope composition and dolomitization fluids in the Feixianguan formation of Triassic, eastern Sichuan of China. Acta Pet. Sin. 22 (8), 2123–2132 (in Chinese).
Jiang, S., Zhang, Y., Huang, W., et al., 2019. Geochemical characteristics of Ordovician strontium isotope in the Ordos basin. Acta Geol. Sin. 93 (11), 2889–2903. https://doi.org/10.19762/j.cnki.dizhixuebao.2019196 (in Chinese).
Jiu, B., Huang, W., Mu, N., et al., 2021. Types and controlling factors of ordovician paleokarst carbonate reservoirs in the southeastern Ordos Basin, China. J. Petrol. Sci. Eng. 198, 108162. https://doi.org/10.1016/j.petrol.2020.108162.
Jones, B., Manning, D.A.C., 1994. Comparison of geochemical indices used for the interpretation of paleoredox conditions in ancient mudstones. Chem. Geol. 114, 111–129. https://doi.org/10.1016/0009-2541(94)90085-X.
Kah, L.C., Thompson, C.K., Henderson, M.A., et al., 2016. Behavior of marine sulfur in the ordovician. Palaeogeogr. Palaeoclimatol. Palaeoecol. 458, 133–153. https://doi.org/10.1016/j.palaeo.2015.12.028.
Konhauser, K.O., Planavsky, N.J., Hardisty, D.S., et al., 2017. Iron formations: a global record of Neoarchaean to Palaeoproterozoic environmental history. Earth Sci. Rev. 172, 140–177. https://doi.org/10.1016/j.earscirev.2017.06.012.
Krabbenhöft, A., Eisenhauer, A., Böhm, F., et al., 2010. Constraining the marine strontium budget with natural strontium isotope fractionations ($^{87}Sr/^{86}Sr^*$, $\delta^{88/86}Sr$) of carbonates, hydrothermal solutions, and river waters. Geochem. Cosmochim. Acta 74 (14), 4097–4109. https://doi.org/10.1016/j.gca.2010.04.009.
Kump, L.R., Arthur, M.A., Patzkowsky, M.E., et al., 1999. A weathering hypothesis for glaciation at high atmospheric pCO_2 during the Late Ordovician. Palaeogeogr. Palaeoclimatol. Palaeoecol. 152, 173–187. https://doi.org/10.1016/S0031-0182(99)00046-2.
Land, L.S., 1983. The application of stable isotopes to studies of the origin of dolomite and to problems of diagenesis of clastic sediments. Stable isotopes in sedimentary geology. SEPM Short. Course 10, 4, 1–4.22.
Lash, G.G., 2018. Significance of stable carbon isotope trends in carbonate concretions formed in association with anaerobic oxidation of methane (AOM), Middle and Upper Devonian shale succession, western New York State, USA. Mar. Petrol. Geol. 91, 470–479. https://doi.org/10.1016/j.marpetgeo.2018.01.032.
Leslie, S.A., Saltzman, M.R., Bergström, S.M., et al., 2011. Conodont biostratigraphy and stable isotope stratigraphy across the Ordovician Knox/Beekmantown unconformity in the central Appalachians. In: Gutiérrez-Alonso, G., Diego, G.B. (Eds.), Ordovician of the World. Publicaciones del Instituto Geológicoy Minero de España.
Li, C., Wu, H., Chu, Z., et al., 2019. Precise determination of radiogenic Sr and Nd isotopic ratios and Rb, Sr, Sm, Nd elemental concentrations in four coal ash and coal fly ash reference materials using isotope dilution thermal ionization mass spectrometry. Microchem. J. 146, 906–913. https://doi.org/10.1016/j.microc.2019.02.034.
Li, B., 2020. Characteristic and identification of diagenetic facies of low permeability and ultra-low permeability dolostone reservoirs: a case study from Ma55 to Ma51 submembers of the Majiagou Formation, central-eastern Ordos Basin. Thiesis, Northwest University, pp. 1–175 (in Chinese).
Li, W., Tu, J., Zhang, J., et al., 2017. Accumulation and potential analysis of self-sourced natural gas in the ordovician Majiagou Formation of Ordos Basin, NW China. Petrol. Explor. Dev. 44 (4), 552–562. https://doi.org/10.1016/S1876-3804(17)30064-2.
Lottermoser, B.G., 1992. Rare earth elements and hydrothermal ore formation processes. Ore Geol. Rev. 7 (1), 25–41. https://doi.org/10.1016/0169-1368(92)90017-F.
Marriott, C.S., Henderson, G.M., Crompton, R., et al., 2004. Effect of mineralogy, salinity, and temperature on Li/Ca and Li isotope composition of calcium carbonate. Chem. Geol. 212 (1–2), 5–15. https://doi.org/10.1016/j.chemgeo.2004.08.002.
Marenco, P.J., Marenco, K.N., Lubitz, R.L., et al., 2013. Contrasting long-term global and short-term local redox proxies during the Great Ordovician Biodiversification Event: a case study from Fossil Mountain, Utah, USA. Palaeogeogr. Palaeoclimatol. Palaeoecol. 377, 45–51. https://doi.org/10.1016/j.palaeo.2013.03.007.
Meidla, T., Ainsaar, L., Backman, J., et al., 2004. Middle–upper ordovician carbon isotope record from västergötland (Sweden) and east Baltic. In: Hints, O., Ainsaar, L. (Eds.), WOGOGOB-2004 Conference Materials. Tartu University Press, Tartu, pp. 67–68.
Nothdurft, L.D., Webb, G.E., Kamber, B.S., 2004. Rare earth element geochemistry of Late Devonian Reefal carbonates, Canning Basin, Western Australia: confirmation of a seawater REE proxy in Ancient limestones. Geochem. Cosmochim. Acta 68 (2), 263–283. https://doi.org/10.1016/S0016-7037(03)00422-8.
Pan, X., Wang, Z., Li, Q., et al., 2020. Sedimentary environments and mechanism of organic matter enrichment of dark shales with low TOC in the Mesoproterozoic Cuizhuang Formation of the Ordos Basin: evidence from petrology, organic geochemistry, and major and trace elements. Mar. Petrol. Geol. 122, 104695. https://doi.org/10.1016/j.marpetgeo.2020.104695.
Pohl, A., Donnadieu, Y., Hir, G.L., et al., 2014. Effect of Ordovician paleogeography on the (in) stability of the climate. Clim. Past 10 (6), 2053–2066. https://doi.org/10.5194/cp-10-2053-2014.
Prasanta, K.M., Sarada, P.M., 2021. Geochemistry of carbonate rocks of the chilpi group, Bastar craton, India: implications on ocean paleoredox conditions at the late paleoproterozoic era. Precambrian Res. 353, 106023. https://doi.org/10.1016/j.precamres.2020.106023.
Qi, J.Z., Guo, M., 2017. Analysis of major controlling factor for hydrocarbon accumulation in ordovician Majiagou Formation in northeastern Ordos Basin. Special Oil Gas Reservoirs 24 (4), 54–59 (in Chinese).
Qiang, L., 2019. Geochemistry of Sedimentary Rocks of Ordovician in SW Ordos and its Paleoceanographic and Palaeoclimatologic Implications. Thesis. Lanzhou University, pp. 1–38 (in Chinese).
Ren, Y., Zhong, D., Gao, C., et al., 2017. High-resolution carbon isotope records and correlations of the lower cambrian Longwangmiao Formation (stage 4, Toyonian) in chongqing, South China. Palaeogeogr. Palaeoclimatol. Palaeoecol. 485, 572–592. https://doi.org/10.1016/j.palaeo.2017.07.013.
Ren, Y., Zhong, D., Gao, C., et al., 2019. The paleoenvironmental evolution of the cambrian Longwangmiao Formation (stage 4, Toyonian) on the Yangtze platform, South China: petrographic and geochemical constrains. Mar. Petrol. Geol. 100, 391–411. https://doi.org/10.1016/j.marpetgeo.2018.10.022.
Rimmer, S.M., 2004. Geochemical paleoredox indicators in devonian-Mississippian black shales, central Appalachian basin (USA). Chem. Geol. 206, 373–391. https://doi.org/10.1016/j.chemgeo.2003.12.029.
Sarangi, S., Mohanty, S.P., Barik, A., 2017. Rare earth element characteristics of Paleoproterozoic cap carbonates pertaining to the Sausar Group, Central India: implications for ocean paleoredox conditions. J. Asian Earth Sci. 148, 31–50. https://doi.org/10.1016/j.jseaes.2017.08.016.
Saltzman, M.R., Edwards, C.T., 2017. Gradients in the carbon isotopic composition of Ordovician shallow water carbonates: a potential pitfall in estimates of ancient CO_2 and O_2. Earth Planet Sci. Lett. 454, 46–54. https://doi.org/10.1016/j.epsl.2017.02.011.
Sarkar, A., Sarangi, S., Ebihara, A., et al., 2003. Carbonate geochemistry across the Eocene/Oligocene Boundary of Kutch, Western India: implications to oceanic O_2-poor condition and foraminiferal extinction. Chem. Geol. 201 (3–4), 281–293. https://doi.org/10.1016/S0009-2541(03)00238-9.
Schmitz, B., Bergström, S.M., Wang, X.F., 2010. The middle Darriwilian (Ordovician) $\delta^{13}C$ excursion (MDICE) discovered in the Yangtze Platform succession in China: implications of its first recorded occurrences outside Baltoscandia. J. Geol. Soc. 167, 249–259. https://doi.org/10.1144/0016-76492009-080.
Sepkoski, J., 1995. The Ordovician radiations: diversification and extinction shown by global genus-level taxonomic data. In: Cooper, J.D., Droser, M.L., Finney, S.C. (Eds.), Ordovician Odyssey: Short Papers for the Seventh International Symposium on the Ordovician System. SEPM, California, pp. 393–396.
Shu, P.C., Feng, Q.H., Xu, S.M., et al., 2021. Model of weathering crust karstification in the ordovician, western Ordos Basin. Acta Sedimentol. Sin. 39 (6), 1565–1579. https://doi.org/10.14027/j.issn.1000-0550.2021.073 (in Chinese).
Su, Z.T., Chen, H.D., Xu, F.Y., et al., 2012. REE characters of the Majiagou dolomites in Ordos Basin. J. Jilin Univ. (Earth Sci. Ed.) 42 (2), 53–61. https://doi.org/10.13278/j.cnki.jjuese.2012.s2.035 (in Chinese).
Sverjensky, D.A., 1984. Europium redox equilibria in aqueous solution. Earth Planet Sci. Lett. 67, 70–78. https://doi.org/10.1016/0012-821X(84)90039-6.
Trotter, J.A., Williams, I.S., Barnes, C.R., et al., 2008. Did cooling oceans rrigger Ordovician biodiversification? Evidence from conodont thermometry. Science

321 (5888), 550–554. https://doi.org/10.1126/science.1155814.
Tu, J., Dong, Y., Zhang, B., et al., 2016. Discovery of effective scale source rocks of the Ordovician Majiagou Fm in the Ordos Basin and its geological significance. Nat. Gas. Ind. B 3, 330–338. https://doi.org/10.1016/j.ngib.2016.12.009.
Vasconcelos, C., McKenzie, J.A., Warthmann, R., et al., 2005. Calibration of the $\delta^{18}O$ paleo-thermometer with dolomite formed in microbial cultures and natural environments. Geology 33, 317–320. https://doi.org/10.1130/G20992.1.
Viehmann, S., Bau, M., Hoffmann, J.E., et al., 2015. Geochemistry of the Krivoy Rog Banded Iron Formation, Ukraine, and the impact of peak episodes of increased global magmatic activity on the trace element composition of Precambrian seawater. Precambrian Res. 270, 165–180. https://doi.org/10.1016/j.precamres.2015.09.015.
Vollstaedt, H., Eisenhauer, A., Wallmann, K., et al., 2014. The Phanerozoic $\delta^{88/86}Sr$ record of seawater: new constraints on past changes in oceanic carbonate fluxes. Geochem. Cosmochim. Acta 128, 249–265. https://doi.org/10.1016/j.gca.2013.10.006.
Warren, J., 2000. Dolomite: occurrence, evolution and economically important associations. Earth Sci. Rev. 52, 1–18. https://doi.org/10.1016/S0012-8252(00)00022-2.
Wang, E.Z., Feng, Y., Guo, T.L., et al., 2022a. Oil content and resource quality evaluation methods for lacustrine shale: a review and a novel three-dimensional quality evaluation model. Earth–Sci. Rev. 232, 104134. https://doi.org/10.1016/j.earscirev.2022.104134.
Wang, E.Z., Li, C.R., Feng, Y., et al., 2022. Novel method for determining the oil moveable threshold and an innovative model for evaluating the oil content in shales. Energy 239 (A), 121848. https://doi.org/10.1016/j.energy.2021.121848.
Wang, J., Wu, S., Li, Q., et al., 2020. Characterization of the pore-throat size of tight oil reservoirs and its control on reservoir physical properties: a case study of the Triassic tight sandstone of the sediment gravity flow in the Ordos Basin, China. J. Petrol. Sci. Eng. 186, 106701. https://doi.org/10.1016/j.petrol.2019.106701.
Wang, Y., Shi, Z.J., Qing, H.R., et al., 2021. Petrological characteristics, geochemical characteristics, and dolomite model of the lower Cambrian Longwangmiao Formation in the periphery of the Sichuan Basin, China. J. Petrol. Sci. Eng. 202, 108432. https://doi.org/10.1016/j.petrol.2021.108432.
Wang, Z., Zhou, H., Wang, X., et al., 2015. Ordovician geological events group in the west and south Ordos Basin. Acta Geol. Sin. 89 (11), 1990–2004 (in Chinese).
Webb, G.E., Kamber, B.S., 2000. Rare earth elements in Holocene reefal microbialites: a new shallow seawater proxy. Geochem. Cosmochim. Acta 64 (9), 1557–1565. https://doi.org/10.1016/S0016-7037(99)00400-7.
Webby, B.D., Paris, F., Droser, M.L., et al., 2004. The Great Ordovician Biodiversification Event, vols. 10–78. Columbia University Press, New York.
Wu, R., Calner, M., Lehnert, O., et al., 2018. Conodont biostratigraphy and carbon isotope stratigraphy of the middle ordovician (darriwilian) Komstad limestone, southern Sweden. Gff 140 (1), 44–54. https://doi.org/10.1080/11035897.2018.1435561.
Xiao, D., Cao, J., Tan, X., et al., 2021. Marine carbonate reservoirs formed in evaporite sequences in sedimentary basins: a review and new model of epeiric basin-scale moldic reservoirs. Earth Sci. Rev. 223, 103860. https://doi.org/10.1016/j.earscirev.2021.103860.
Xie, R.C., Zhou, W., Zhang, C., et al., 2020. Characteristics, influencing factors, and prediction of fractures in weathered crust karst reservoirs: a case study of the Ordovician Majiagou Formation in the Daniudi Gas Field, Ordos Basin, China. Geol. J. 55, 7790–7806. https://doi.org/10.1002/gj.3907.
Xiong, Y., Li, L., Wen, C.X., et al., 2016. Characteristics and genesis of ordovician $Ma5^{1+2}$ sub-member reservoir in northeastern Ordos Basin. Oil Gas Geol. 37 (5), 691–701. https://doi.org/10.11743/ogg20160509 (in Chinese).
Xiong, Y., Tan, X., Zhong, S., et al., 2022. Dynamic paleokarst geochemistry within 130 Myr in the middle ordovician shanganning carbonate platform, North China. Palaeogeogr. Palaeoclimatol. Palaeoecol. 591, 110879. https://doi.org/10.1016/j.palaeo.2022.110879.
Xu, W., Li, J., Liu, X., et al., 2021. Accumulation conditions and exploration directions of Ordovician lower assemblage natural gas, Ordos Basin, NW China. Petrol. Explor. Dev. 48 (3), 641–654. https://doi.org/10.1016/S1876-3804(21)60051-4.
Yang, X., 2011. Study on the Carbonate Reservoir Characteristics of Majiagou Formation in Daniudi Area, Ordos Basin. Thesis, Xi'an Shiyou University, pp. 1–19 (in Chinese).
Young, S.A., Saltzman, M.R., Ausich, W.I., et al., 2010. Did changes in atmospheric CO_2 coincide with latest Ordovician glacial-interglacial cycles? Palaeogeogr. Palaeoclimatol. Palaeoecol. 296 (3–4), 376–388. https://doi.org/10.1016/j.palaeo.2010.02.033.
Young, S.A., Gill, B.C., Edwards, C.T., et al., 2016. Middle–Late Ordovician (Darriwilian–Sandbian) decoupling of global sulfur and carbon cycles: isotopic evidence from eastern and southern Laurentia. Palaeogeogr. Palaeoclimatol. Palaeoecol. 458, 118–132. https://doi.org/10.1016/j.palaeo.2015.09.040.
Yu, C., Cui, J., 2019. Geochemical characteristics and genesis of dolomite in Majiagou Ma55 submember of the Northeast Yishan Slope, Ordos Basin. Earth Sci. 44 (8), 2761–2774. https://doi.org/10.3799/dqkx.2019.954 (in Chinese).
Zhang, J.T., Jin, X.H., Li, S.J., et al., 2016. Types and origin of pore-fillings from the 5^{th} member of the ordovician Majiagou Formation in Ordos Basin. Oil Gas Geol. 37 (5), 684–690. https://doi.org/10.11743/ogg20160508 (in Chinese).
Zhang, J.T., He, Z.L., Yue, X.J., et al., 2017. Genesis of iron-rich dolostones in the 5^{th} member of the Majiagou Formation of the ordovician in Ordos Basin. Oil Gas Geol. 38 (4), 776–783. https://doi.org/10.11743/ogg20170414 (in Chinese).
Zhang, T., Shen, Y., Algeo, T.J., 2010. High-resolution carbon isotopic records from the ordovician of South China: links to climatic cooling and the Great ordovician biodiversification event (GOBE). Palaeogeogr. Palaeoclimatol. Palaeoecol. 289, 102–112. https://doi.org/10.1016/j.palaeo.2010.02.020.
Zhang, Y., Zhan, R., Zhen, Y., et al., 2019. Ordovician integrative stratigraphy and timescale of China. Sci. China Earth Sci. 62, 61–88. https://doi.org/10.1007/s11430-017-9279-0.
Zhao, Z., Sun, Y., Li, C., et al., 2015. Stratigraphic division and correlation of ordovician system in Ordos Basin. Special Oil Gas Reservoirs 22 (5), 9–17 (in Chinese).